autotrophic flagellates (2–20 μm), consumed by micro and mesozooplankton; picoplankton (0.2–2 μm), consumed by heterotrophic nanoflagellates; and inedible phytoplankton >20 μm. The uptake of nutrients (NO_3, NH_4 and PO_4) have been decoupled from the carbon assimilation processes by including dynamic nutrient kinetics[22], whereby nutrient uptake is dependent on both the level of intercellular storage and external nutrient concentrations. The microbial food web contains bacteria, heterotrophic flagellates and microzooplankton, each with dynamically varying C:N:P ratios and is described in ref. 23. Bacteria consume DOC, decompose detritus and can compete for inorganic nutrients with phytoplankton. Heterotrophic flagellates feed on bacteria and picoplankton and are consumed by microzooplankton and mesozooplankton. Microzooplankton feed on diatoms, autotrophic and heterotrophic flagellates and are consumed by mesozooplankton. Mesozooplankton feed on diatoms, autotrophic flagellates and microzooplankton[24]. All three grazer groups are cannibalistic.

Simulations were made with the ERSEM parameter sets used in ref. 15, for the Humber plume region of the North Sea. The model was forced by heat fluxes calculated from meteorological data observed at Dublin. Although data for Dublin are not from the North Sea, Dublin lies directly in the path of weather systems which commonly move from the Gulf Stream to the North Sea.

Received 25 September 2001; accepted 24 January 2002.

1. Mysterud, A., Stenseth, N. C., Yoccoz, N. G., Langvain, R. & Steinhelm, G. Nonlinear effects of large-scale climatic variability on wild and domestic herbivores. *Nature* **410,** 1096–1099 (2001).
2. Sugihara, G., Grenfell, B. & May, R. M. Distinguishing error from chaos in ecological time series. *Phil. Trans. R. Soc. Lond. B* **330,** 235–251 (1990).
3. Berryman, A. A. & Millstein, J. A. Are ecological systems chaotic—and if not, why not? *Trends Evol. Ecol.* **4(1),** 26–28 (1989).
4. Cane, M. A., Eshel, G. & Buckland, R. W. Forecasting Zimbabwean maize yield using eastern equatorial Pacific sea surface temperature. *Nature* **370,** 204–205 (1994).
5. Shackleton, N. J. The 100,000-year ice-age cycle identified and found to lag temperature, carbon dioxide and orbital eccentricity. *Science* **289,** 1897–1902 (2000).
6. Taylor, A. H., Colebrook, J. M., Stephens, J. A. & Baker, N. G. Latitudinal displacements of the Gulf Stream and the abundance of plankton in the north-east Atlantic. *J. Mar. Biol. Assoc. UK* **72,** 919–921 (1992).
7. Taylor, A. H. North-south shifts of the Gulf Stream and their climatic connection with the abundance of zooplankton in the UK and its surrounding seas. *ICES J. Mar. Sci.* **52,** 711–721 (1995).
8. Glover, R. S. The continuous plankton recorder survey of the North Atlantic. *Symp. Zool. Soc. Lond.* **19,** 189–210 (1967).
9. Frid, C. L. J. & Huliselan, N. V. Far field control of long term changes in Northumberland (NW North Sea) coastal zooplankton. *ICES J. Mar. Sci.* **53(6),** 972–977 (1996).
10. Taylor, A. H. in *Changing States of Large Marine Ecosystems of the North Atlantic* (eds Sherman, K. & Skjoldal, H.-R.) (in the press).
11. George, D. G. The impact of regional-scale changes in the weather on long-term dynamics of *Eudaptomus* and *Daphnia* in Esthwaite Water, Cumbria. *Freshwat. Biol.* **45,** 111–121 (2000).
12. George, D. G. & Taylor, A. H. UK lake plankton and the Gulf Stream. *Nature* **378,** 139 (1995).
13. Hurrell, J. W. Decadal trends in the North Atlantic Oscillation: regional temperatures and precipitation. *Science* **269,** 67600679 (1995).
14. Allen, J. I., Blackford, J. C. & Radford, P. J. A 1-D vertically resolved modelling study of the ecosystem dynamics of the middle and southern Adriatic Sea. *J. Mar. Sys.* **18,** 265–286 (1998).
15. Allen, J. I., Howland, R. M. H., Bloomer, N. & Uncles, R. J. Simulating the spring phytoplankton bloom in the Humber Plume, UK. *Mar. Poll. Bull.* **37,** 295–305 (1999).
16. Baretta, J. W., Ebanhoh, W. & Ruardij, P. (eds) The european regional seas ecosystem model II. *J. Sea Res.* **38(3/4),** 229–483 (1997).
17. Blumberg, A. F. & Mellor, G. L. in *Mathematical Modelling of Estuarine Physics (Proc. Int. Symp. Hamburg, 1978)* (eds Sunderland & Holtz) 203–214 (Springer, Berlin, 1980).
18. Taylor, A. H. North-south shifts of the Gulf Stream: ocean-atmosphere interactions in the North Atlantic. *Int. J. Climatol.* **16,** 559–583 (1996).
19. Colebrook, J. M. Continuous plankton records: overwintering and annual fluctuations in the abundance of zooplankton. *Mar. Biol.* **84,** 261–265 (1985).
20. Huisman, J., van Oostven, P. & Weissing, F. J. Critical depth and critical turbulence: Two different mechanisms for the development of phytoplankton blooms. *Limnol. Oceanogr.* **44(7),** 1781–1787 (1999).
21. Ebenhöh, W., Baretta, J. W. & Baretta-Bekker, J. G. The primary production module in a marine ecosystem model ERSEM II. *J. Sea Res.* **38,** 173–194 (1997).
22. Droop, M. R. The nutrient status of algal cells in continuous culture. *J. Mar. Biol. Assoc. UK* **54,** 825–855 (1974).
23. Baretta-Bekker, J. G., Baretta, J. W., Hansen, A. S. & Riemann, B. An improved model of carbon and nutrient dynamics in the microbial food web in marine enclosures. *Aquat. Microb. Ecol.* **14,** 91–108 (1998).
24. Broekhuizen, N. R., Heath, M. R., Hay, S. G. & Gurney, S. C. Modelling the dynamics of the North Sea's mesozooplankton. *Neth. J. Sea Res.* **33,** 381–406 (1995).

Acknowledgements

We wish to thank J. Stephens and J. Dearman for assisting with the calculations. B. Clarke provided statistical advice. A.H.T. is a Fellow of the Sir Alister Hardy Foundation for Ocean Science, which provided the plankton data. This work is part of the Core Strategic Programme of Plymouth Marine Laboratory.

Competing interests statement

The authors declare that they have no competing financial interests.

Correspondence and requests for materials should be addressed to A.H.T. (e-mail: aht@pml.ac.uk).

Direct visuomotor transformations for reaching

Christopher A. Buneo, Murray R. Jarvis, Aaron P. Batista* & Richard A. Andersen

Division of Biology, California Institute of Technology, Mail Code 216-76, Pasadena, California 91125, USA

The posterior parietal cortex (PPC) is thought to have a function in the sensorimotor transformations that underlie visually guided reaching, as damage to the PPC can result in difficulty reaching to visual targets in the absence of specific visual or motor deficits[1]. This function is supported by findings that PPC neurons in monkeys are modulated by the direction of hand movement, as well as by visual, eye position and limb position signals[2–9]. The PPC could transform visual target locations from retinal coordinates to hand-centred coordinates by combining sensory signals in a serial manner to yield a body-centred representation of target location[10–12], and then subtracting the body-centred location of the hand. We report here that in dorsal area 5 of the PPC, remembered target locations are coded with respect to both the eye and hand. This suggests that the PPC transforms target locations directly between these two reference frames. Data obtained in the adjacent parietal reach region (PRR) indicate that this transformation may be achieved by vectorially subtracting hand location from target location, with both locations represented in eye-centred coordinates.

The problem that we address here is shown in Fig. 1a. Although the execution of movement requires the specification of a detailed pattern of inputs to the muscles, movement planning is believed to involve the computation of higher level movement parameters, such as the direction and/or distance that the hand must move to reach the target (vector *M*)[10]. This is due to the fact that movement goals, as well as evidence of our success in achieving these goals, are largely expressed in high level terms, that is, as visually perceived discrepancies between the position of the hand and target or deviations from a desired path[13]. Hereafter we use the term 'target position in hand coordinates' to describe vector *M* in Fig. 1a, although the terms 'movement vector' and 'motor error' could also be used. This information could be derived by subtracting the sensed location of the hand (vector *H*) from the sensed location of the target (vector *T*), as long as hand position and target position are coded in a common frame of reference. However, although target position appears to be coded in eye-centred (retinal) coordinates in the early stages of reach planning[14], hand position is derived from both visual and proprioceptive signals, and can conceivably be coded in eye-centred coordinates, body centred coordinates (that is, with respect to the torso), or both. It is unclear therefore whether the operation shown in Fig. 1a is achieved by subtracting the position of the hand from the position of the target directly, using eye-centred coordinates (Fig. 1a, b), or by transforming target locations from eye- to head- to body-centred coordinates, and then subtracting the body-centred position of the hand[10,11] (Fig. 1c).

We have approached this problem by analysing the reach-related activity of neurons in the PPC, while varying target position, hand position and gaze direction. Single cell recordings were obtained from area 5 (Fig. 2a, b), a subdivision of the PPC that projects directly to cortical and subcortical motor structures[15–17]. In an initial experiment, 89 neurons from two monkeys were studied under four experimental conditions (Fig. 2c). In two conditions, gaze was held constant at the centre position of a vertically oriented

* Present address: Howard Hughes Medical Institute, and Department of Neurobiology, Stanford University School of Medicine, Fairchild Building, Room D209, Stanford, California 94305, USA

board of push buttons, and initial hand location was varied to the left (condition 1) or right (condition 2) of this centre position. In the other two conditions, initial hand location was located at the centre position and gaze was varied either to the left (condition 3) or right (condition 4) of centre. Across the four conditions, mean firing rate varied least when target locations were identical in both hand and eye coordinates. For example, the activity of the neuron in Fig. 2 varied substantially between conditions 1 and 2, when target locations were identical in hand coordinates but different in both body coordinates (with respect to the torso) and eye coordinates (with respect to the fixation point). The activity of this neuron also varied substantially between conditions 3 and 4, when target locations were identical in hand and body coordinates but different in eye coordinates. However, activity was very similar between conditions 1 and 4 and between conditions 2 and 3, when target locations were identical in both hand and eye coordinates.

This point is shown more generally in Fig. 3a–e. In each scatterplot, individual data points correspond to the mean firing rate of a single cell for two movements to the same target location in hand, body, eye, body and hand, or eye and hand coordinates (panels a–e, respectively). Data from all cells and all possible target locations are shown. The scatter in each plot illustrates how well that particular coordinate frame or frames accounted for area 5 neuronal population activity. A low degree of scatter (that is, a high degree of correlation) indicates a good fit to the data, whereas a high degree of scatter (low correlation) indicates a poor fit. Statistical analyses of the data in Fig. 3 revealed that area 5 activity was best correlated when target locations were identical in both eye and hand coordinates (Kruskal–Wallis test with nonparametric multiple comparisons, $P < 0.05$).

Although the data in Fig. 3 could by explained by the presence of two populations of neurons, one coding in eye coordinates and the other in hand coordinates, Fig. 4 shows that the responses of neurons in area 5 are more consistent with a single population coding target location in both reference frames. Figure 4a–d shows the responses of an idealized neuron coding target location in eye coordinates (panels a, b), both eye and hand coordinates (panel c) or hand coordinates (panel d). Figure 4a shows that if target locations are coded purely in eye coordinates, tuning curves for target location in eye coordinates will not shift when initial hand location in eye coordinates is varied, although they will modulate in amplitude if initial hand location in eye coordinates is explicitly coded, as in Fig. 4b. Figure 4d shows that if target locations are coded purely in hand coordinates, tuning curves will shift completely with initial hand location. However, Fig. 4c shows that if target locations are coded in both eye and hand coordinates, tuning

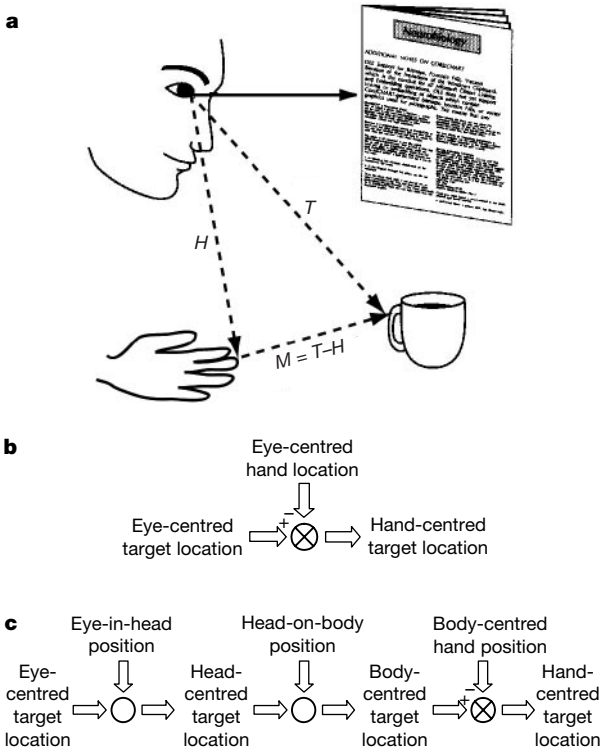

Figure 1 Visuomotor transformation schemes. **a**, Example of reaching for a cup while fixating on a newspaper. The position of the cup is initially represented in the brain in terms of its location on the peripheral retina (*T*). To reach for the cup, its position with respect to the hand must be known (*M*). This information could be acquired by directly subtracting hand position (*H*) from target position (*T*) in eye coordinates (**a**, **b**), or by gradually transforming the position of the target from eye- to body-centred coordinates, and subtracting the body-centred position of the hand (**c**). (Adapted from ref. 29.)

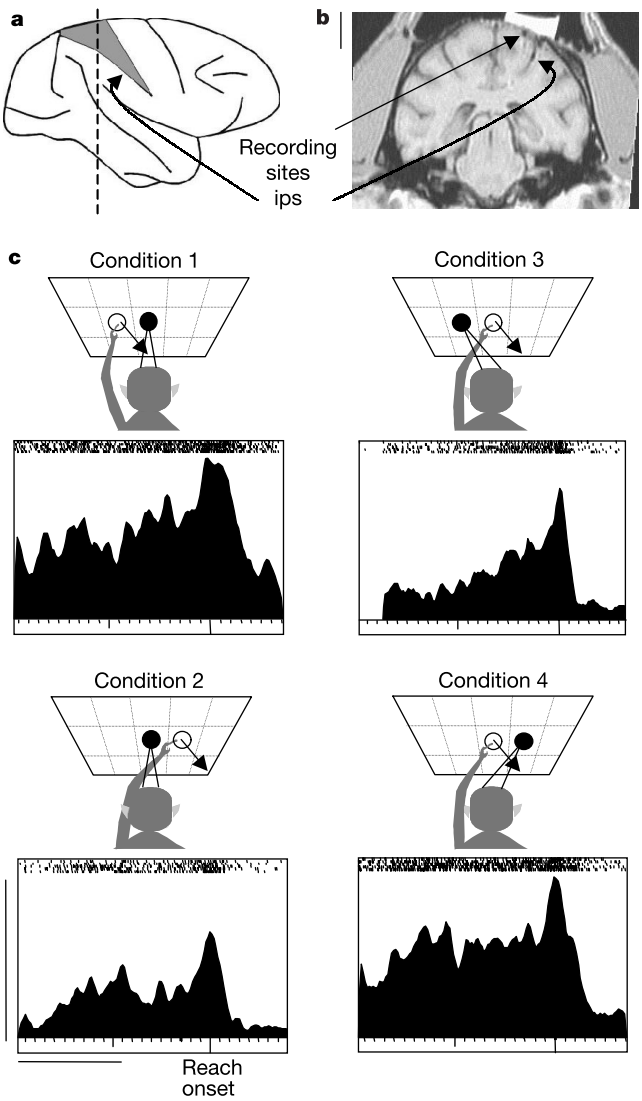

Figure 2 Responses of a single neuron from area 5. **a**, Diagram of a macaque monkey brain showing the location of area 5 (shaded region) and the approximate location of the magnetic resonance image (MRI) section in **b**. ips, intraparietal sulcus. **b**, Coronal T1-weighted MRI section through the approximate centre of the area 5 recording sites. Scale bar, 1 cm. **c**, Spike density histograms of the activity of one area 5 neuron for the same planned movement vector (down and to the right) in each of four experimental conditions. Vertical scale bar, 140 spikes s^{-1}; horizontal scale bar, 1 s.

curves for identical target locations in eye coordinates will partially shift with initial hand location, reflecting a 'compromise' between the eye and hand reference frames. Figure 4e shows for area 5 ($N = 89$) the distribution of tuning curve shifts when target locations in eye coordinates were the same and initial hand location was varied from left to right by 36°. This distribution has a single large peak at 18°(standard error ±3), corresponding to a partial shift and consistent with a simultaneous coding of target location in both eye and hand coordinates. For comparison, Fig. 4e shows the same analysis applied to the PRR data ($N = 98$) of ref. 14. This distribution has a large peak at 0°, corresponding to no shift and consistent with a purely eye-centred coding of target location.

To explore further the hypothesis that neurons in area 5 code target location in both eye and hand coordinates, we trained one monkey to reach to a row of five targets from each of five starting locations, while maintaining fixation at a single board location (one position to the right of centre, see Fig. 5a). This design was chosen so that responses of area 5 neurons could be compared directly with the responses predicted by the different coding models in Fig. 4. Figure 5b shows a contour plot of data obtained from one area 5 neuron in this experiment. These contours have a largely oblique orientation, similar to those of the idealized neuron in Fig. 4c. To facilitate comparisons between real response fields and their idealized counterparts, we summarized the trends giving rise to such contours by calculating the gradient of each response field and taking its resultant (see Methods for definition). The vector field superimposed on the contour plot in Fig. 5b shows the gradient that was obtained for this neuron. The resultant of the gradient in Fig. 5b is shown in Fig. 5c (blue vector) along with a 'population resultant' derived from 15 area 5 neurons (black vector), and the gradient resultant obtained for the idealized neuron in Fig. 4c (red vector). The resultants derived from experimental data have an orientation very similar to the one derived from the idealized responses, pointing largely down and to the right, which is consistent with a

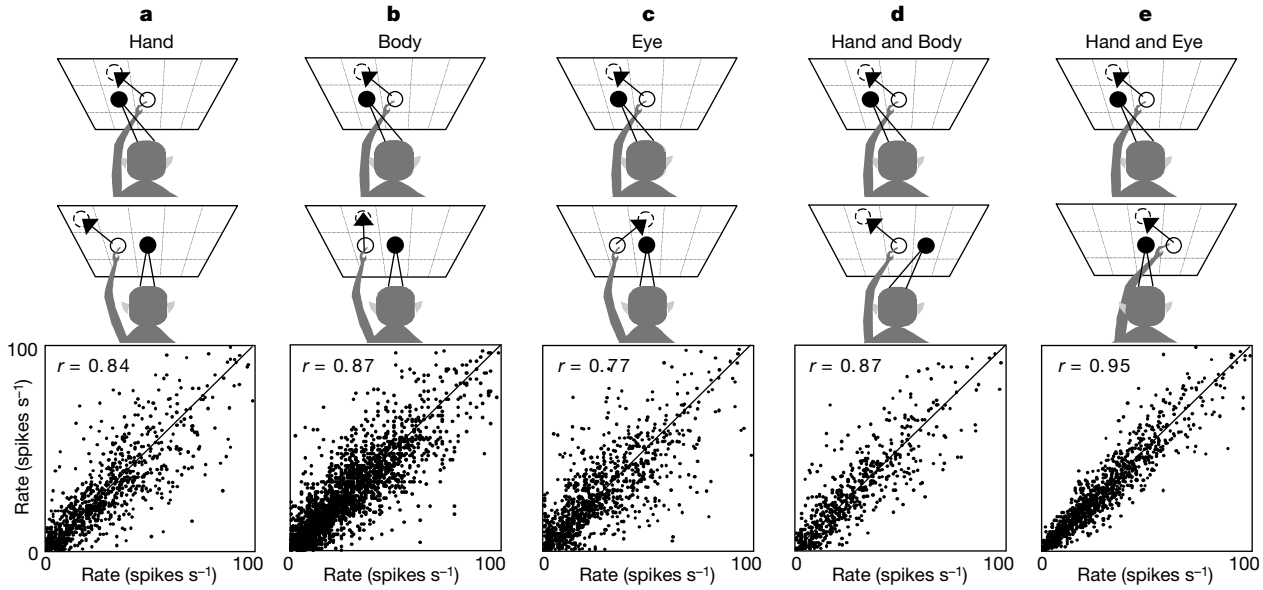

Figure 3 Area 5 neuronal population activity for reaches to identical target locations in hand coordinates (**a**), body coordinates (**b**), eye coordinates (**c**), hand and body coordinates (**d**), and hand and eye coordinates (**e**). Each data point corresponds to a cell's firing rate for a pair of movements; movements in a pair were taken from different experimental conditions and were randomly assigned to the ordinate or abscissa. Example experimental conditions used to construct each figure (as well as an example pair of movements) are shown above the scatterplots.

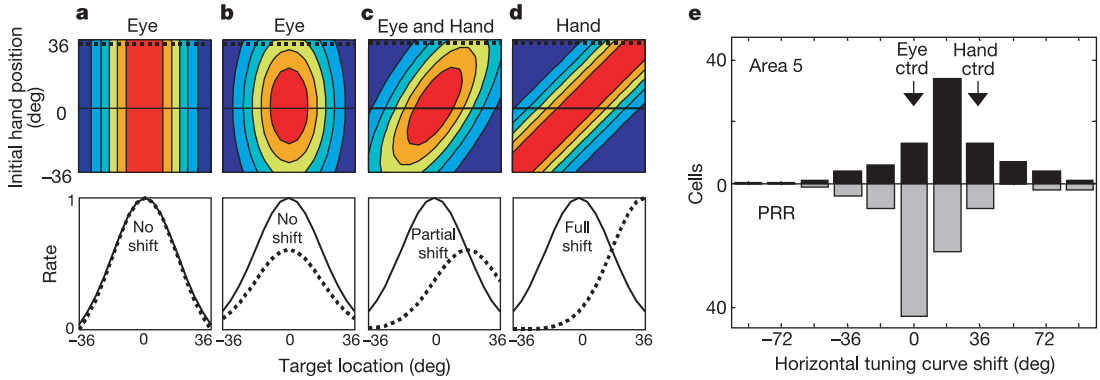

Figure 4 Shifting and non-shifting response fields in the PPC. **a**–**c**, Responses of an idealized neuron coding target location in eye coordinates (**a**), target location and initial hand location in eye coordinates (**b**), target location in eye and hand coordinates (**c**), and target location in hand coordinates (**d**). Responses are plotted as a function of horizontal target location and horizontal initial hand location in eye coordinates. Tuning curves below each contour plot represent slices though each response field at initial hand locations of 0° (black line) and 36° (dotted line). **e**, Distribution of horizontal tuning curve 'shifts' for area 5 and PRR[14].

coding of target location in both eye and hand coordinates. For comparison, Fig. 5d, e shows data obtained from PRR in the same experiment. The contours in Fig. 5d appear most similar to the idealized neuron in Fig. 4b, that is, they appear consistent with a coding of target location and initial hand location in eye coordinates. The gradient resultant for this neuron is shown in Fig. 5e (blue vector), along with a population resultant derived from 17 PRR neurons (black vector) and the resultant obtained for the idealized neuron in Fig. 4b (red vector). All three resultants point largely to the right in Fig. 5e, consistent with a coding of target location in eye coordinates.

The present results indicate that remembered target locations are coded in both eye and hand coordinates in area 5. These results are not unique to the perireach epoch—similar results were obtained when activity occurring immediately after presentation of the target, as well as during the delay period, was analysed separately. Thus, reaching to remembered target locations seems to entail a direct transformation from eye-centred to hand-centred coordinates, although more indirect schemes (for example, Fig. 1c) may still operate in other contexts[18]. The responses of neurons in the PRR suggest a mechanism for this direct transformation. Although PRR neurons strongly code target location in eye coordinates, some cells are 'gain modulated'[19] by initial hand location (for example, see Fig. 5d), which is also coded in eye coordinates in this area[20]. If both target location and initial hand location are coded in eye coordinates in the PPC, then they can simply be subtracted to compute the target's location in hand coordinates, as shown in Fig. 1a, b. A role for the PPC in the comparison of target and hand position-related signals has been previously suggested[21,22], although the coordinate frame underlying this operation has not been specified until now. Simulations have shown that this operation can be implemented neurally by a simple, weighted summation of gain-modulated neurons like those found in the PRR (Fig. 5d)[23].

The fact that target locations are coded in both eye and hand coordinates in area 5 might mean that further processing is needed to complete the transformation to hand coordinates. However, it is also quite possible that this spatial representation is necessary for the functions performed by this cortical area, and therefore does not signify an intermediate step in the transformation process[24]. Consistent with this latter possibility are the findings that area 5 receives visual, proprioceptive, and efference copy signals[2–9], which are probably represented in different coordinate frames[25]. In principle, the gain-modulated cells in the PRR can be used to compute target locations purely in hand-centred coordinates, that is, without an eye-centred component, by weighting the convergence of activity differently. Such a scheme may be used to construct representations in other brain areas that are more heavily biased towards hand-centred coordinates than the one observed in area 5. □

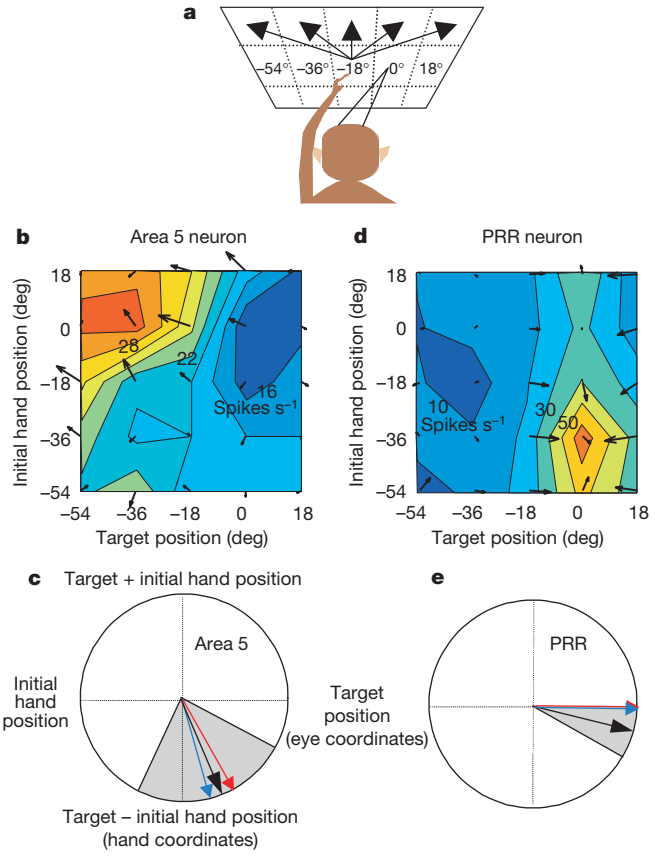

Figure 5 Results from the second experiment. **a**, Task schematic. **b**, Contour plot and gradient (black vectors) for one area 5 neuron. **c**, Resultant of the gradient in **b** (blue vector), population resultant of 15 single cell resultants (black vector), and gradient resultant for the idealized neuron in Fig. 4c (red vector). The shaded region indicates the 95% confidence interval for the population resultant[27]. **d**, Contour plot and gradient for a PRR neuron. **e**, Resultant of the gradient in **d** (blue vector), resultant of 17 PRR single cell resultants (black vector), and gradient resultant for the idealized neuron in Fig. 4b (red vector).

Methods

Behavioural paradigm and neurophysiological recordings

Reaches were made to touch sensitive buttons that were 3.7 cm in diameter and set 7.5 cm apart, within a board placed 24 cm from the monkeys. In each condition, reaches were typically made to between 8 and 11 buttons located immediately surrounding the initial hand position and/or within an adjacent column of buttons (Fig. 2). Each button contained both a red and a green light-emitting diode (LED). The red LED instructed the animals where to direct and maintain their gaze, whereas the green LED instructed the animals where to place their hand. All trials began with the illumination of both a red and a green LED. A green (target) LED at another location was then briefly illuminated (300 ms duration). After a delay period of 600–1,000 ms, the LEDs instructing the initial hand location and fixation point were turned off and the animal reached to the remembered location of the target in complete darkness while maintaining fixation. Eye position was monitored using the scleral search coil technique. Reaching movements were made with the contralateral (left) arm.

We obtained recordings from the right hemispheres of two monkeys (*Macaca mulatta*). Eighty-nine area 5 neurons (61 from the animal CKY and 28 from animal DNT) were studied in all four conditions of the initial experiment. Furthermore, we studied 15 area 5 neurons and 17 PRR neurons (all from animal CKY) in the second experiment. The approximate centre of the PRR recording sites in this second experiment was 5-mm posterior to the centre of the area 5 sites, at depths below the superficial cortex. These sites represent only a portion of the larger reach-related region reported in an earlier study[26]. All analyses were performed on the mean firing rate (5 repetitions) during a 400-ms epoch centred on movement onset.

Correlation analysis

Determination of statistical differences among correlations was facilitated by constructing a distribution of correlation coefficients ($N = 200$) for each coordinate frame(s), using standard statistical bootstrapping techniques[27]. A Kruskal–Wallis test with nonparametric multiple comparisons ($P < 0.05$) was then performed on these distributions[28], which revealed that area 5 activity was best correlated when target locations were identical in both eye and hand coordinates (Fig. 3e).

At the population level, activity was generally well correlated in all reference frames, due in part to the fact that area 5 neurons exhibit relatively broad spatial tuning as well as the fact that cells with low firing rates tended to fire at low rates in all experimental conditions. To assess the degree to which our findings depended on the relative number of low firing pairs in Fig. 3a–e, we performed an additional analysis of the scatter in these plots, using a measure that is relatively insensitive to differing numbers of low-firing pairs and data points (which varied across Fig. 3a–e). More specifically, scatter (s) was quantified as

$$s = \sum_{i=1}^{n} \rho_i^2 \Big/ \sum_{i=1}^{n} r_i^2 \qquad (1)$$

where ρ is the perpendicular distance to the unity line, and r is the distance to the origin. This analysis gave the same result as that which was obtained using the correlation coefficient, that is, scatter was least when target locations were identical in both eye and hand coordinates (Kruskal–Wallis test with nonparametric multiple comparisons, $P < 0.05$).

Idealized neural responses

The mean firing rates (*fr*) of the idealized neurons shown in Fig. 4a–d, are given by equation (2) (from top to bottom, respectively):

$$fr = e^{-\left(\frac{T^2}{2}\right)}$$

$$fr = e^{-\left(\frac{T^2}{2} + \frac{H^2}{8}\right)} \qquad (2)$$

$$fr = e^{-\left(\frac{T^2}{4} + \frac{(T-H)^2}{4}\right)}$$

$$fr = e^{-\frac{(T-H)^2}{2}}$$

where T is the horizontal position of the target in eye coordinates, H is the horizontal position of the hand in eye coordinates, and $T - H$ is the horizontal position of the target in hand coordinates (see Fig. 1a). Our observations regarding these responses appear to be insensitive to both the form of these functions (gaussian versus sigmoid) as well as the nature of their interaction (multiplicative versus additive).

Gradient analysis

We estimated gradients from the data using an approximate numerical method (Matlab; Mathworks). The gradient resultant is a measure of the 'orientation' of an individual response field, and hence is an indicator of the variable or variables to which a neuron is most responsive (target position, initial hand position, and so on), regardless of the form of tuning (gaussian, sigmoid, and so on). To account for symmetrically shaped response fields we doubled the angles of the gradient vectors, then subtracted 360° from those angles greater than or equal to 360°, before taking the resultant[28]. This procedure transformed the data in such a way that resultants could be expressed easily in terms of their dependence on target position and initial hand position, as well as their sum and difference (Fig. 5c, e). Resultants could not, however, be mapped directly onto the response fields from which they were derived. For example, although neurons coding target position purely in hand-centred coordinates have obliquely oriented response fields (Fig. 4d), as points along the unity line correspond to identical hand-centred target positions, their gradient resultants would be expected to point straight down in Fig. 5c, e. Single cell and population resultants were normalized to unit length before plotting in Fig. 5.

Received 3 September 2001; accepted 25 January 2002.

1. Rondot, P., Recondo, J. & de Ribadeau Dumas, J. Visuomotor ataxia. *Brain* **100,** 355–376 (1977).
2. Kalaska, J. F., Caminiti, R. & Georgopoulos, A. P. Cortical mechanisms related to the direction of two-dimensional arm movements—relations in parietal area 5 and comparison with motor cortex. *Exp. Brain Res.* **51,** 247–260 (1983).
3. Georgopoulos, A. P., Caminiti, R. & Kalaska, J. F. Static spatial effects in motor cortex and area 5: quantitative relations in a two-dimensional space. *Exp. Brain Res.* **4,** 446–454 (1984).
4. Kalaska, J. F., Cohen, D. A. D., Prud'homme, M. & Hyde, M. L. Parietal area 5 neuronal activity encodes movement kinematics, not movement dynamics. *Exp. Brain Res.* **80,** 351 (1990).
5. Lacquaniti, F., Guignon, E., Bianchi, L., Ferraina, S. & Caminiti, R. Representing spatial information for limb movement: role of area 5 in the monkey. *Cerebr. Cortex* **5,** 391–409 (1995).
6. Kalaska, J. F. & Crammond, D. J. Deciding not to go: neuronal correlates of response selection in a go/nogo task in primate premotor and parietal cortex. *Cerebr. Cortex* **5,** 410–428 (1995).
7. Scott, S. H., Sergio, L. H. & Kalaska, J. F. Reaching movements with similar hand paths but different arm orientations. II. Activity of individual cells in dorsal premotor cortex and parietal area 5. *J. Neurophysiol.* **78,** 2413–2426 (1997).
8. Graziano, M. S. A., Cooke, D. F. & Taylor, C. S. R. Coding the location of the arm by sight. *Science* **290,** 1782–1786 (2000).
9. Battaglia-Mayer, A. *et al.* Early coding of reaching in the parietooccipital cortex. *J. Neurophysiol.* **83,** 2374–2391 (2000).
10. Flanders, M., Tillery, S. I. H. & Soechting, J. F. Early stages in a sensorimotor transformation. *Behav. Brain Sci.* **15,** 309–320 (1992).
11. Henriques, D. Y. P., Klier, E. M., Smith, M. A., Lowy, D. & Crawford, J. D. Gaze-centered remapping of remembered visual space in an open-loop pointing task. *J. Neurosci.* **18,** 1583–1594 (1998).
12. McIntyre, J., Stratta, F. & Lacquaniti, F. Short-term memory for reaching to visual targets: psychophysical evidence for body-centered reference frames. *J. Neurosci.* **18,** 8423–8435 (1998).
13. Jordan, M. I. & Rumelhart, D. E. Forward models: supervised learning with a distal teacher. *Cognitive Sci.* **16,** 307–354 (1992).
14. Batista, A. P., Buneo, C. A., Snyder, L. H. & Andersen, R. A. Reach plans in eye-centered coordinates. *Science* **285,** 257–260 (1999).
15. Strick, P. L. & Kim, C. C. Input to primate motor cortex from posterior parietal cortex (area 5). I. Demonstration by retrograde transport. *Brain Res.* **157,** 325–330 (1978).
16. Wiesendanger, R., Wiesendanger, M. & Ruegg, D. G. An anatomical investigation of the corticopontine projection in the primate (*Macaca fascicularis* and *Saimiri sciureus*). II. The projection from the frontal and parietal areas. *Neuroscience* **4,** 747–765 (1979).
17. Petrides, M. & Pandya, D. N. Projections to the frontal cortex from the posterior parietal region in the rhesus monkey. *J. Comp. Neurol.* **228,** 105–116 (1984).
18. Carozza, M., McIntyre, J., Zago, M. & Lacquaniti, F. Viewer-centered and body-centered frames of reference in direct visuomotor transformations. *Exp. Brain Res.* **129,** 201–210 (1999).
19. Andersen, R. A., Essick, G. K. & Siegel, R. M. Encoding of spatial location by posterior parietal neurons. *Science* **230,** 456–458 (1985).
20. Buneo, C. A., Batista, A. P. & Andersen, R. A. Frames of reference for reach-related activity in two parietal areas. *Soc. Neurosci. Abstr.* **24,** 262 (1998).
21. Desmurget, M. *et al.* Role of the posterior parietal cortex in updating reaching movements to a visual target. *Nature Neurosci.* **2,** 563–567 (1999).
22. Bullock, D., Cisek, P. & Grossberg, S. Cortical networks for control of voluntary arm movements under variable force conditions. *Cerebr. Cortex* **8,** 48–62 (1998).
23. Salinas, E. & Abbott, L. Transfer of coded information from sensory to motor networks. *J. Neurosci.* **15,** 6461–6474 (1995).
24. Deneve, S., Latham, P. E. & Pouget, A. Efficient computation and cue integration with noisy population codes. *Nature Neurosci.* **4,** 826–831 (2001).
25. Moran, D. W. & Schwartz, A. B. Motor cortical representation of speed and direction during reaching. *J. Neurophysiol.* **82,** 2676–2692 (1999).
26. Snyder, L. H., Batista, A. P. & Andersen, R. A. Coding of intention in the posterior parietal cortex. *Nature* **386,** 167–170 (1997).
27. Effron, B. & Tibshirani, R. J. *An Introduction to the Bootstrap* (Chapman & Hall, New York, 1993).
28. Zar, J. H. *Biostatistical Analysis* (Prentice-Hall, Upper Saddle River, New Jersey, 1999).
29. Andersen, R. A., Snyder, L. H., Li, C. S. & Stricanne, B. Coordinate transformations in the representation of spatial information. *Curr. Opin. Neurobiol.* **3,** 171–176 (1993).

Acknowledgements

This work was supported by the Defense Advanced Research Projects Agency (DARPA), the National Eye Institute, the Sloan-Schwartz Center for Theoretical Neurobiology, the James G. Boswell Foundation and an NIH training grant fellowship to C.A.B. We thank B. Gillikin and V. Shcherbatyuk for technical assistance; D. Dubowitz for collecting and processing the MRI data; J. Baer and J. Wynne for veterinary care; and C. Reyes-Marks for administrative assistance. We also thank J. Boline and K. Shenoy for comments.

Competing interests statement

The authors declare that they have no competing financial interests.

Correspondence and requests for materials should be addressed to R.A.A. (e-mail: andersen@vis.caltech.edu).

Chondroitinase ABC promotes functional recovery after spinal cord injury

Elizabeth J. Bradbury*, Lawrence D. F. Moon†§, Reena J. Popat*, Von R. King‡, Gavin S. Bennett*, Preena N. Patel*, James W. Fawcett† & Stephen B. McMahon*

** Sensory Function Group, Centre for Neuroscience Research, Hodgkin Building, Kings College London, Guy's Campus, London Bridge, London SE1 1UL, UK*
† Department of Physiology and Centre for Brain Repair, University of Cambridge, Robinson Way, Cambridge CB2 2PY, UK
‡ Department of Neuroscience, St Bartholomew's and the Royal London School of Medicine and Dentistry, Queen Mary, University of London, Mile End Road, London E1 4NS, UK

The inability of axons to regenerate after a spinal cord injury in the adult mammalian central nervous system (CNS) can lead to permanent paralysis. At sites of CNS injury, a glial scar develops, containing extracellular matrix molecules including chondroitin sulphate proteoglycans (CSPGs)[1,2]. CSPGs are inhibitory to axon growth *in vitro*[3–5], and regenerating axons stop at CSPG-rich regions *in vivo*[6]. Removing CSPG glycosaminoglycan (GAG) chains attenuates CSPG inhibitory activity[7–10]. To test the functional effects of degrading chondroitin sulphate (CS)-GAG after spinal cord injury, we delivered chondroitinase ABC (ChABC) to the lesioned dorsal columns of adult rats. We show that intrathecal treatment with ChABC degraded CS-GAG at the injury site, upregulated a regeneration-associated protein in injured neurons, and promoted regeneration of both ascending sensory projections and descending corticospinal tract axons. ChABC treatment also restored post-synaptic activity below the lesion after electrical stimulation of corticospinal neurons, and promoted functional recovery of locomotor and proprioceptive behaviours. Our results demonstrate that CSPGs are important

§ Present address: Miami Project to Cure Paralysis, 1095 NW 14th Terrace, PO Box 16960, Mail Locator R-48, Miami, Florida 33101, USA.